Nuclear Materials and Energy 10 (2017) 1–8

Contents lists available at ScienceDirect

Nuclear Materials and Energy

journal homepage: www.elsevier.com/locate/nme

The influence of annealing on yttrium oxide thin film deposited by reactive magnetron sputtering: Process and microstructure

Y. Mao*, J. Engels, A. Houben, M. Rasinski, J. Steffens, A. Terra, Ch. Linsmeier, J.W. Coenen

Forschungszentrum Jülich GmbH, Institut für Energie- und Klimaforschung - Plasmaphysik, Partner in the Trilateral Euregio Cluster, 52425 Jülich, Germany

ARTICLE INFO

Article history:
Received 12 September 2016
Available online 26 January 2017

Keywords:
Yttrium oxide
Reactive magnetron sputtering
Annealing
Microstructure
Permeation barrier
Composite interface

ABSTRACT

Yttrium oxide thin films were prepared by reactive magnetron sputtering in different deposition condition with various oxygen flow rates. The annealing influence on the yttrium oxide film microstructure is investigated. The oxygen flow shows a hysteresis behavior on the deposition rate. With a low oxygen flow rate, the so called metallic mode process with a high deposition rate (up to 1.4 µm/h) was achieved, while with a high oxygen flow rate, the process was considered to be in the poisoned mode with an extremely low deposition rate (around 20 nm/h). X-ray diffraction (XRD) results show that the yttrium oxide films that were produced in the metallic mode represent a mixture of different crystal structures including the metastable monoclinic phase and the stable cubic phase, while the poisoned mode products show a dominating monoclinic phase. The thin films prepared in metallic mode have relatively dense structures with less porosity. Annealing at 600 °C for 15 h, as a structure stabilizing process, caused a phase transformation that changes the metastable monoclinic phase to stable cubic phase for both poisoned mode and metallic mode. The composition of yttrium oxide thin films changed from nonstoichiometric to stoichiometric together with a lattice parameter variation during annealing process. For the metallic mode deposition however, cracks were formed due to the thermal expansion coefficient difference between thin film and the substrate material which was not seen in poisoned mode deposition. The yttrium oxide thin films that deposited in different modes give various application options as a nuclear material.

1. Introduction

Yttrium oxide is an industrially and technologically very useful ceramic material under its several advanced properties: good thermal and chemical stability, high mechanical strength and hardness [1-3]. Also yttrium oxide has a wide application in nuclear research because of its low activation due to neutron irradiation [4].

Yttrium oxide exhibits several structural polymorphisms: C-cubic (Ia3), B-monoclinic (C2/m), A-hexagonal (P32m) and H-hexagonal ($P6_3/mmc$). The cubic phase is stable at room temperature, which transforms to H-hexagonal phase at ~2327 °C or to B-monoclinic phase at ~10 GPa [5-8]. Therefore, in low temperature region (<2327 °C), the cubic phase, as the stable phase, is normally preferred.

One option for producing the yttrium oxide thin film is to use reactive magnetron sputtering deposition. Using the reactive magnetron sputtering process to produce compound material has been well investigated, especially the influence of the amount of the reactive gas on the deposition process and thin film properties [9-12]. In reactive magnetron sputtering of yttrium oxide, a hysteresis of the deposition parameters as a function of the oxygen flow is often reported. At low oxygen flow the deposition rate is quite high, and therefore only little yttrium oxide compound is formed on the target and this regime is referred to as the metallic mode. At high oxygen flow the target becomes more oxidized, and the deposition rate decreases. This regime is called the poisoned mode.

Recent research by Lei et al. [12] demonstrated that, for yttrium oxide deposition, metallic mode and poisoned mode give different phases, which are the cubic phase and the monoclinic phase, respectively. Comparing to poisoned mode thin films, the yttrium oxide coatings deposited in metallic mode have a relatively dense structure, less porosity and larger grain size and are considered a preferred coating due to their superior mechanical properties. Nevertheless, this conclusion still needs to be confirmed for nuclear application (high temperature application), for which the annealing becomes a necessary post treatment for the sputtered yttrium oxide thin film to reach the stable structure. Therefore this work

* Corresponding author.
E-mail address: y.mao@fz-juelich.de (Y. Mao).

http://dx.doi.org/10.1016/j.nme.2016.12.031

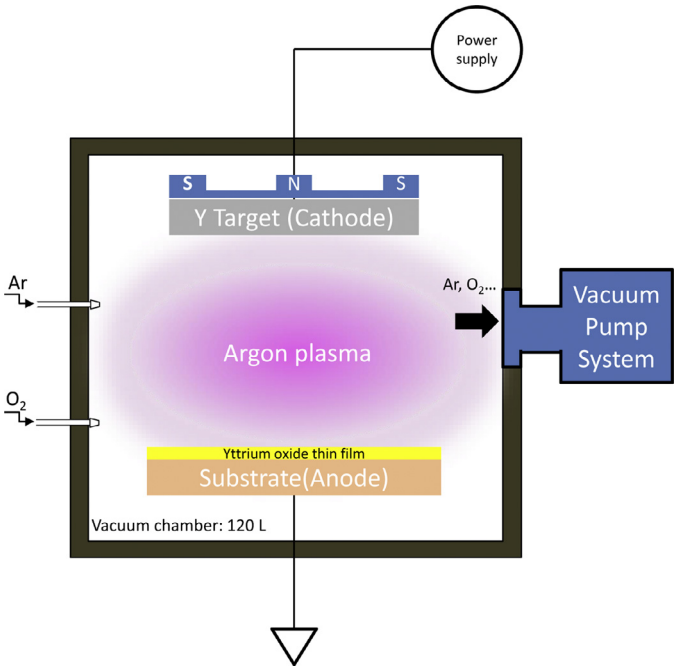

Fig. 1. The magnetron sputtering setup.

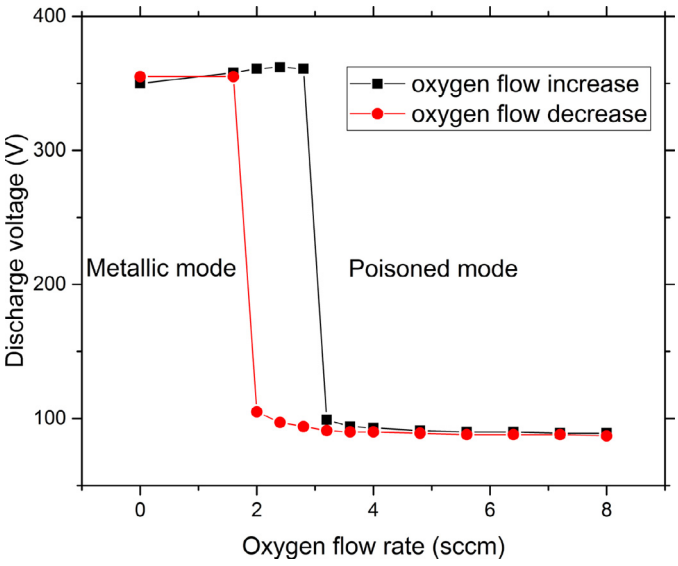

Fig. 2. Oxygen flow influence on discharge voltage at 350 W RF power supply.

investigates further the post-annealing influence on the reactive magnetron sputtered yttrium oxide thin film microstructure.

2. Experimental techniques

2.1. Deposition and annealing

The yttrium oxide thin films were deposited by a Prevac magnetron sputtering system (Fig. 1) on the polished P92 steel (0.07%–0.13% C; 0.3%–0.6% Mn; max 0.02% P; max 0.01% S; max 0.5% Si; 8.5%–9.5% Cr; 0.3%–0.6% Mo; 0.15%–0.25% V; 0.03%–0.07% N; max 0.4% Ni; max 0.02% Al; 0.04%–0.09% Nb; 1.5%–2% W; 0.001–0.006% B; max 0.01% Ti; max 0.01% Zr) substrates with the microstructure of martensite. It is a substitute for the potential fusion reactor structural material, EUROFER. The magnetron target material was yttrium metal (Kurt J. Lesker Company, 99.9% purity, 76.2 mm diameter, 6.35 mm thickness). The distance between the target and the substrate is ~15 cm. Argon was used to generate the plasma. Oxygen was injected as reactive gas, so that yttrium oxide compound could be formed. The oxygen inlet position was away from the target, around the sample stage. An RF power supply with 13.45 MHz frequency was used to avoid the arcing effect of DC power supply [9,13]. The deposition power was 350 W. In a single deposition process several substrates were placed on the sample stage, which rotated with a speed of 20 °/s during the deposition process to guarantee the homogeneous distribution of the deposition. The substrate temperature during deposition was about 140 °C due primarily to the kinetic energy and heat of condensation of coating atoms and plasma radiation. The oxygen flow changed between 2 standard cubic centimeter per minute (sccm) and 10 sccm measured by a gas flow controller. The Ar flow rate was constant 25 sccm in all cases. The vacuum chamber background pressure was $\sim 5 \times 10^{-8}$ mbar and the pressure during deposition was $\sim 6.5 \times 10^{-3}$ mbar. The pumping speed was 212 L/s.

After deposition, some samples were annealed at 600 °C for 15 h by using a vacuum tube furnace. The pressure in the vacuum tube furnace during annealing was $\sim 1 \times 10^{-5}$ mbar. The average heating rate and cooling rate were ~4 °C/min and ~1.7 °C/min, respectively.

2.2. Characterization

To calculate the deposition rate of each process, the exact yttrium oxide film thickness after deposition was measured by using a Dektak 6 M profilometer. The microstructure of the films was analyzed by a dual beam SEM/FIB (focused ion beam) Carl Zeiss Crossbeam 540 device together with an energy-dispersive X-ray spectroscopy (EDX). A glow discharge optical emission spectroscopy (GD-OES, RF mode with 1.011 kHz frequency and a duty cycle of 0.1, 800 V bias voltage, 3.72 mbar plasma pressure) was utilized to quantitatively measure the thin film composition [14]. Crystallographic properties were measured by a D8 Discovery X-ray Diffractometer (XRD) using Cu-Kα radiation (0.154 nm) in Bragg–Brentano geometry with a 2θ range from 10° to 60°

3. Results and discussion

3.1. Deposition condition and deposition rate

Fig. 2 illustrates the relationship between discharge voltage and the oxygen flow at 350 W RF power supply. This diagram shows a hysteresis behavior as many papers have reported about reactive magnetron sputtering [11-13,15]. When the oxygen flux increases, the discharge voltage firstly remains at a high value over 300 V. When the oxygen flow reaches about 3 sccm, the deposition voltage abruptly drops to a low point, and then remains relatively constant at the low value below 100 V with the further increasing of oxygen flow rate. When the oxygen flux decreases from 8 sccm, firstly the discharge voltage remains at the low value. After the oxygen flow rate decreases to about 2 sccm, the deposition voltage suddenly increases to the high value again, and then remains relatively constant when the oxygen flow rate further decreases.

The high and low discharge voltages correspond to different deposition mechanisms which are the so called metallic mode and poisoned mode, respectively. In metallic mode, mainly the yttrium metal atoms are sputtered from the target, and impinge on the substrate with a reaction with the inject oxygen forming an yttrium oxide thin film. However, during poisoned mode deposition with a high oxygen flux, the increasing excess oxygen can diffuse up to the yttrium metal target forming an yttrium oxide compound layer on the target surface. Sputtering rates from compound targets are less than that of pure metallic target by a factor up to 50 [12]. There are two main reasons: a) the sputtering yield of metal atoms

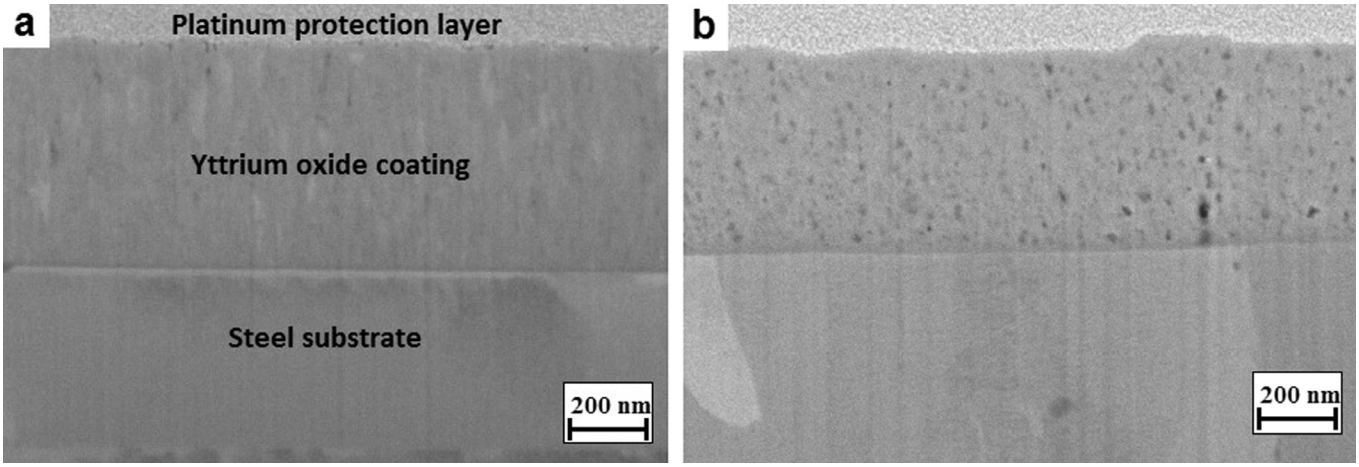

Fig. 3. SEM images of a FIB prepared cross-section for metallic mode (a) and poisoned mode (b) deposition before annealing.

Table. 1
Deposition rates change with different oxygen flow.

Oxygen flow (sccm)	Deposition rate (nm/h)
1.8	1343 ± 26
2	1313 ± 49
3.2	25 ± 2
4	20 ± 2

from a compound on the target surface is less than that of a metallic target; b) compounds have higher secondary electron emission coefficients than metals and hence most of the energy of the incident ions is utilized to breaking bonds with the resultant creation and acceleration of secondary electrons [9-13,16]. The transition of the target from metallic surface to a compound surface is a one-way process and is very difficult to control. If the oxygen gas flow is reduced after the transition, the system does not convert back at the same flow. This is due to the presence of the residual oxide layer on the cathode. To clear the residual oxide layer on the cathode, the reactive gas flow needs to be further reduced. Then the deposition will convert to metallic mode [17]. This is the reason for this hysteresis relationship between the discharge voltage and the oxygen flow rate.

As the deposition rate has a linear relationship to the deposition discharge voltage [13], one can expect that the oxygen flow rate supplied has the same hysteresis influence on the deposition rate. Table 1 shows the deposition rates of these two deposition condition. In a typical metallic mode, a deposition rate up to ~ 1300 nm/h was obtained, while in a typical poisoned mode the value was only ~25 nm/h.

3.2. Microstructure

Because of the different deposition mechanisms, the deposited films in different modes show different microstructures. Fig. 3 represents the SEM images of FIB prepared cross sections for both metallic mode and poisoned mode deposition with 2 sccm oxygen flow and 3.2 oxygen flow, respectively. Comparing the microstructures of these two thin films, the yttrium oxide thin film produced in metallic mode (Fig. 3a) shows a tendency to form columnar structure with dense structure and low porosity which has been often reported [12,18,19]. On the contrary, high porosity was seen in the poisoned mode thin films (Fig. 3b), mainly owing to the low kinetic energy of the deposited atoms and the trap of the gas phase. As reported in several papers [20,21], the momentum flux of the deposited substance shows a high influence on the film density.

After annealing, the microstructure of the thin films produced by both modes are shown in Fig. 4. For the metallic mode thin film (Fig. 4a), a crack formation is visible due to the stress caused by the thermal expansion coefficient difference between the substrate and yttrium oxide thin film. The thermal expansion coefficient of yttrium oxide is 8.1 (10^{-6}/K), while P92 steel/ EUROFER has a thermal expansion coefficient around 12 (10^{-6}/K) [22]. Even though the heating and cooling rate are rather gentle (4 °C/min and 1.7 °C/min), the stress is still sufficient for crack formation. The crack problem in metallic mode after annealing can also be well revealed in Fig. 5. However, for poisoned mode thin films, the stress caused by the thermal expansion coefficient difference is redistributed due to the present of high porosity. In this case, hence, there is no crack formation. Nevertheless, an intermediate layer between the thin film and the substrate is observed in poisoned mode thin film (Fig. 4b). EDX analysis results are presented in Fig. 6 indicating the interlayer composition. The strong signal of Cr and O at the interface region demonstrates a CrO_x formation. A good explanation for this would be the excess oxygen atoms diffuse and react with the Cr from the P92 substrate during the annealing process. This results agree with the composition analysis in Section 3.3.

Fig. 7 illustrates the X-ray diffraction diagrams of the metallic mode thin films (2 sccm oxygen flow rate) before and after annealing, and Fig. 8 shows the poisoned mode case (3.2 sccm oxygen flow rate). For a better view, the background intensity of the annealed thin films were shifted up for 3000 a. u. A mixture of yttrium oxide cubic phase and monoclinic phase can be identified in as-deposited metallic mode thin films. After annealing the metastable monoclinic phase was eliminated. Only the peaks for the stable cubic phase can be observed. This means that there is a phase transformation from the metastable monoclinic phase to the stable cubic phase during annealing process. Also from Fig. 7, the intensity of the peaks get steeper after annealing. By calculating the theoretical minimum grain size based on the well-known Scherrer's formula [23,24], this value changes from 21 ± 0.5 nm to 28 ± 0.6 nm after annealing. This result points to a grain growth during the annealing process. This phase transformation and grain growth of magnetron sputtered films during annealing are frequently reported [25-29]. Additionally, for the metallic mode as-deposited film, the XRD pattern peaks shift to a lower angle comparing with the standard peak positions of the yttrium oxide cubic phase. This is because of the nonstoichiometric composition of the thin film. The excess oxygen atoms stay in the interstitial

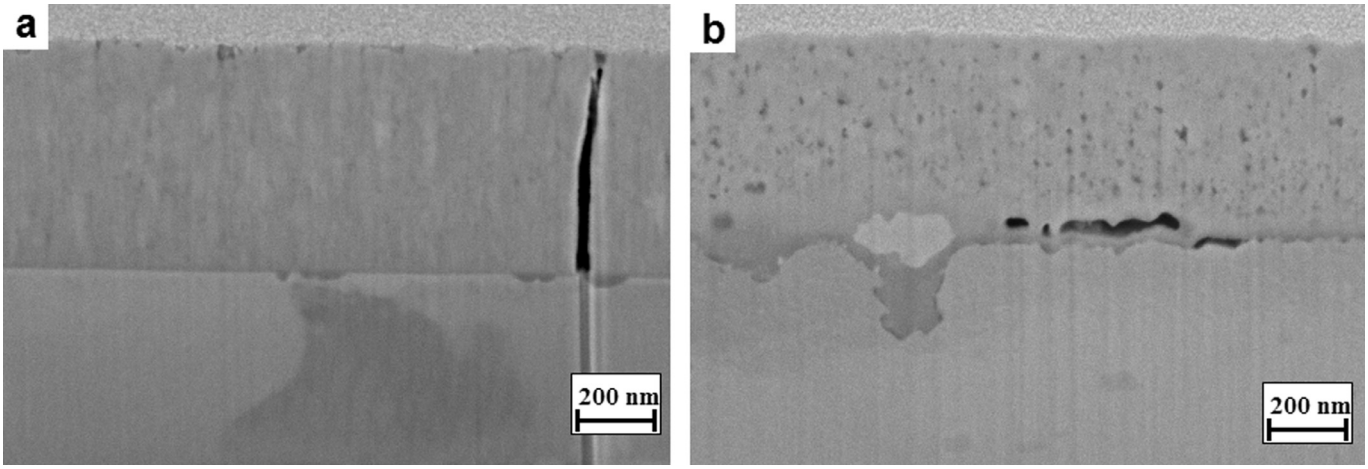

Fig. 4. SEM images of a FIB prepared cross-section for metallic mode (a) and poisoned mode (b) deposition after annealing.

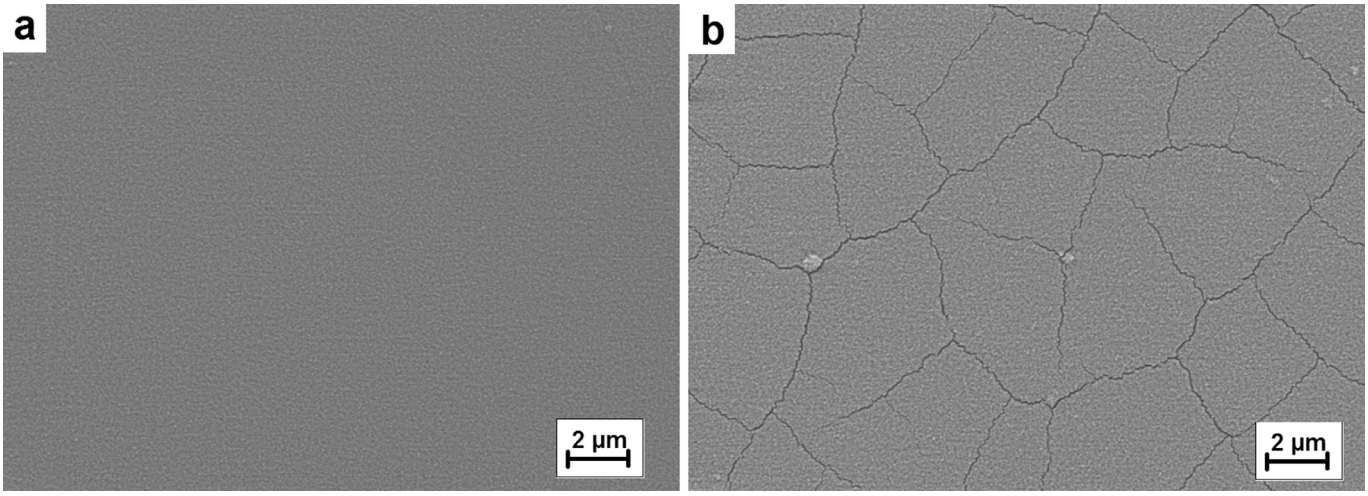

Fig. 5. SEM images of the surface morphology for the metallic mode thin films before (a) and after annealing (b).

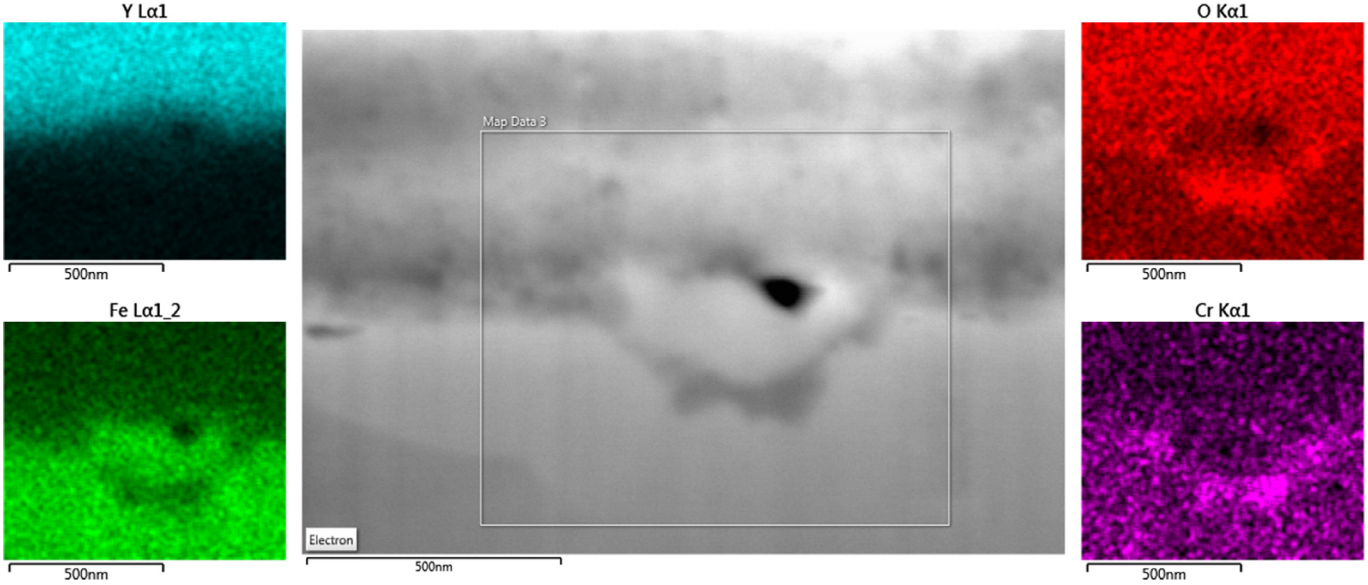

Fig. 6. EDX map of the interlayer for the poisoned mode thin film after annealing.

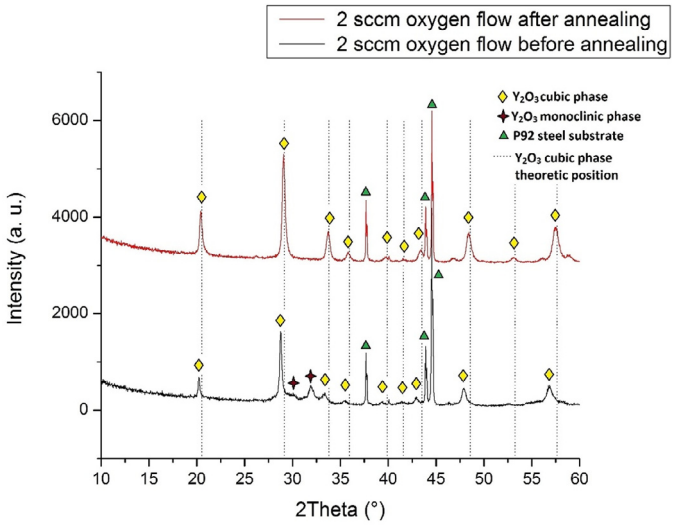

Fig. 7. X-ray diffraction diagrams of the thin films produced with 2 sccm oxygen flow (metallic mode) before and after annealing.

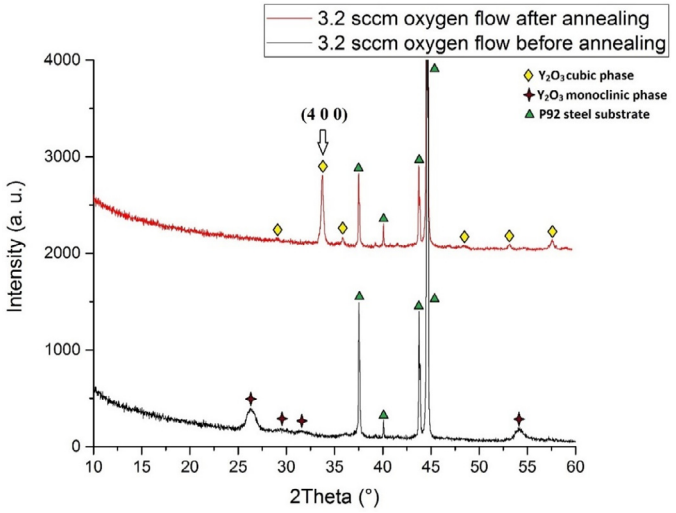

Fig. 8. X-ray diffraction diagrams of yttrium oxide produced by magnetron sputtering with different oxygen flow after annealing.

position of yttrium oxide lattice so that the lattice parameter becomes larger, which corresponds to the peak shifting to the left. While after annealing, the peak shifting gets smaller. Based on the XRD pattern and the Bragg's Law [23], the calculated lattice parameters of the films as deposited and annealed are 10.74 ± 0.02 Å and 10.62 ± 0.01 Å, respectively. This means that the lattice parameter changes back towards the standard value of yttrium oxide (10.604 Å [30]). Because the excess oxygen atoms, which stayed at interstitial lattice position of yttrium oxide, diffuse either to the atmosphere or to the substrate during the annealing process. The diffusion of the excess oxygen during annealing will be further discussed in Section 3.3.

From Fig. 8, the as-deposited poisoned mode thin film represents a clean metastable monoclinic phase. Moreover, the XRD spectrum of the poisoned mode thin film depicts only few peaks showing the monoclinic phase and the peaks are relatively broad. Based on these results, we can assume that the poisoned mode product tends to form a low crystalline structure. This result corresponds to the theory from the structure zone models of reactive magnetron sputtering [18]. When the sputtered atoms with low kinetic energy are deposited on the substrate, they cannot overcome the energy barrier to form the low energy stable structure. This leads to the formation of fine structure and metastable phases. After annealing the metastable monoclinic phase was eliminated during the annealing process. Only the peaks for the stable cubic phase can be observed (Fig. 8). This means there is also a phase transformation from the metastable monoclinic phase to the stable cubic phase during annealing process which is similar with the metallic mode diagrams. Furthermore, the poisoned mode yttrium oxide thin film shows a preferred (4 0 0) orientation after annealing. Possibly, this phenomenon is because of the different ion bombardment condition in poisoned mode deposition; as some articles have noted a change of preferential orientation can be caused by ion bombardment [31,32].

3.3. Composition

The composition depth profiles measured by GDOES are shown in Fig. 9. About the GDOES results details: 1. For all depth profiles, the oxygen concentration in the very beginning - the top layer - is always very high due to: a) The glow discharge source is evacuated to 10^{-2} mbar only, so the vacuum is not very clean. b) Every discharge damages the anode material forming surface porosity. During sample changing, some air will be trapped in the porosity. At the beginning of the next discharge, the trapped air will be released. 2. The thickness of the metallic mode thin film is around 1 µm, while the poisoned mode thin film thickness is around 200 nm. This is the reason why the measuring time for the poisoned mode thin film is significantly shorter. 3. Only three channels are used in the measurement: O, Y and Fe. That is the reason for 100% Fe concentration in the steel substrate. 4. The reference samples for GDOES calibration were a pure Y metal (99.99 w% Y) and a CE 650 sample (from Swerea KIMLAB) with 34 w% oxygen.

It was expected that the oxygen and yttrium would have matched the stoichiometric relationship, which is 3:2 (60%:40%). However, the as-deposited thin films which were produced in both modes have an oxygen concentration higher than 60%. The non-stoichiometric yttrium oxide compound produced by reactive magnetron sputtering has been widely reported in latter papers [1,10,12,33]. Considering also the lattice parameter results from XRD analysis in Section 3.2, this elevated oxygen level points, again, to the trap of the oxygen atoms inside lattice interstitial position. Besides, the voids, grain boundary and other defects of the film are also the possible positions for the excess oxygen atoms. The poisoned mode thin film shows a higher oxygen concentration than the metallic mode thin film because of the higher oxygen flow during magnetron deposition. During the annealing process, the excess oxygen atoms can diffuse to the atmosphere or to the substrate as discussed in Section 3.2. Hence, after annealing the oxygen and yttrium concentration ratio reaches the prescribed values of 60%:40% in the thin film. The diffusion of the excess oxygen agrees with the peak shifting results from the XRD analysis. Furthermore, there is an oxygen peak at the interface between the thin film and the substrate for the poisoned mode thin film after annealing. This proves again the existing of an intermediate oxide layer.

4. Fusion applications

4.1. Permeation barrier

During the fusion reactor operation, tritium atoms have a potential possibility to permeate through the reactor wall or other components of the fusion power plant. This may cause a series of problems, including: fuel loss, tritium accumulation in other parts of the vessel and radiological hazards. In order to suppress the permeation through the reactor walls, a permeation barrier coating is required. In latter research, several materials are considered as the

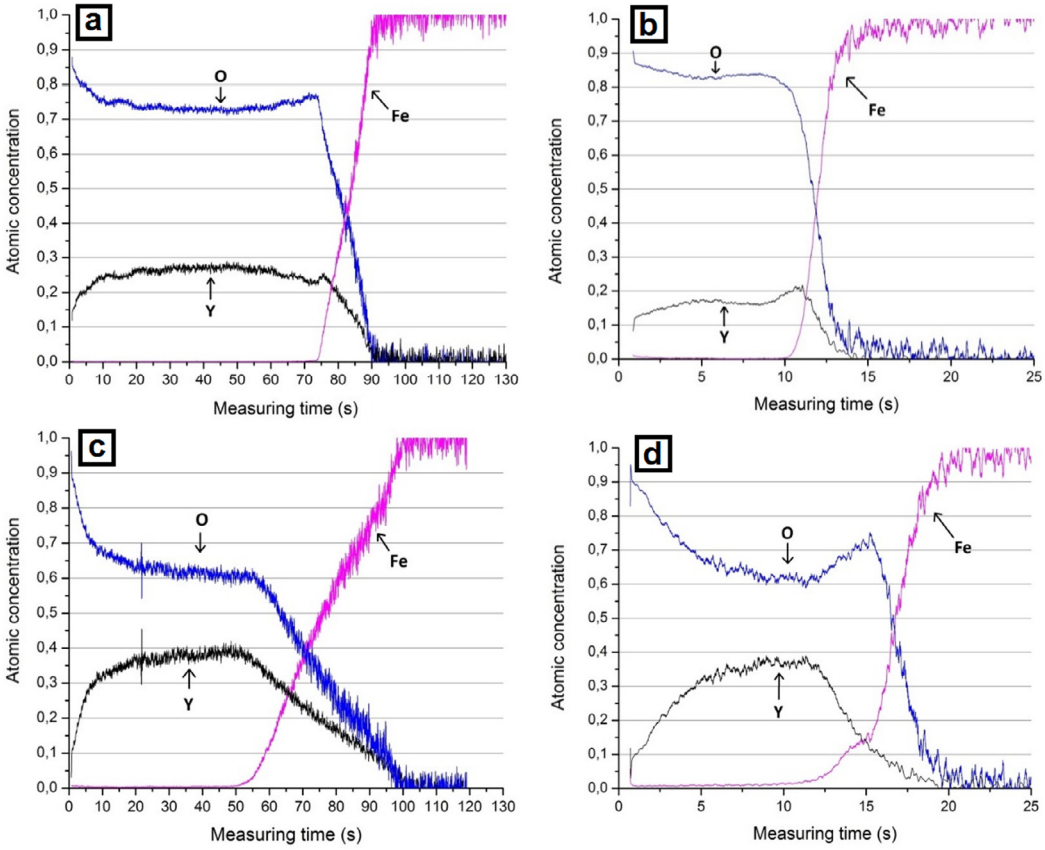

Fig. 9. GDOES depth profile for: metallic mode as-deposited thin film (a); poisoned mode as-deposited thin film (b); metallic mode thin film after annealing (c); poisoned mode thin film after annealing (d).

candidate for permeation barrier, such as Al_2O_3 [34,35], Er_2O_3 [36-38].

Here, yttrium oxide thin film is prepared as a promising candidate for tritium permeation barrier coatings for fusion reactors because of its potentially high permeation reduction factor [39,40].

As the cracks will cause significant impact on the permeation measurement, the crack free poisoned mode yttrium oxide thin films were chosen for the test. The yttrium oxide thin films were deposited on Eurofer97 substrates (0.3 mm thickness, 250 mm diameter plate) in poisoned mode. Then the thin films were annealed at 550 °C for 16 h in the vacuum tube furnace. After that, the longtime permeation measurements on were proceeded over 7 days by Engels et al. [39]. During the measurement, the deuterium filling time is ~20 h. Then the permeation reduction factor stabilized at a value of ~30. The thin film microstructure remained unchanged during annealing at 550 °C in deuterium atmosphere and under the conditions of the permeation measurement [39].

4.2. Interface material for tungsten fiber reinforced tungsten composites

In future fusion reactors, tungsten is a main candidate material for the first wall material of the divertor. The intrinsic brittleness of tungsten is, however, a concern with respect to the fusion environment with high transient heat loads and neutron irradiation. To overcome this drawback, a tungsten fiber-reinforced tungsten (W_f/W) composites are being developed relying on an extrinsic toughing mechanism [41-46]. For W_f/W composites, a weak interface layer between the tungsten fibers and tungsten matrix is required for the required pseudo ductile behavior. Yttrium oxide is an ideal candidate interface material for the W_f/W composite due to its several advanced properties: good thermal and chemical stability, high mechanical strength and hardness. For this application, the yttrium oxide thin films produced in metallic mode were chosen, because of their dense structure and low porosity. Fig. 10 represents the as-deposited yttrium oxide coating on the W fiber.

During the composites manufacturing by powder metallurgy process (consolidation temperature up to 2000 °C), especially during the Field Assisted Sintering Technology (FAST) process, the insulating yttrium oxide interface will get damaged due to external pressure, local overheating and dielectric breakdown effect [47,48]. This interface damaged can be mitigated by increasing the interface thickness. Fig. 11 shows the yttrium oxide interface with different thickness in the actual W_f/W composite after the FAST process [49]. Here, a functional interface region could be established after consolidation with the relatively thick yttrium oxide thin film interface produced by metallic mode deposition.

5. Conclusion

A series of yttrium oxide films, for fusion application, were deposited by magnetron reactive sputtering on P92 steel substrate under different deposition conditions (metallic mode and poisoned mode). In as-deposited thin films, a mixed structure of metastable monoclinic phase and stable cubic phase is formed in metallic mode, while in the poisoned mode, a dominating metastable monoclinic phase is formed. An oxygen composition excess is also observed. As a consequence, to achieve the preferred stable microstructure as a permeation barrier coating, the necessity of the annealing process has been confirmed. Annealing causes a recrystallization and a phase transformation from the metastable monoclinic phase to the stable cubic phase. The thin films, then, reach

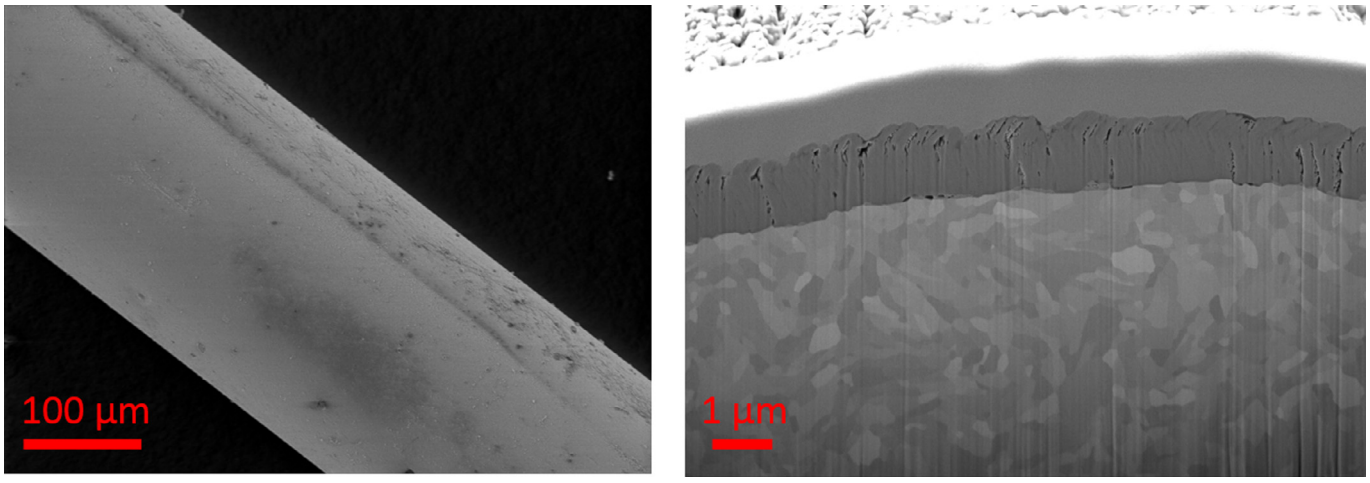

Fig. 10. SEM image of the as-deposited yttrium oxide thin film surface on single tungsten fiber (a); SEM image of the thin film cross section prepared by FIB cut showing yttrium oxide thin film structure (b).

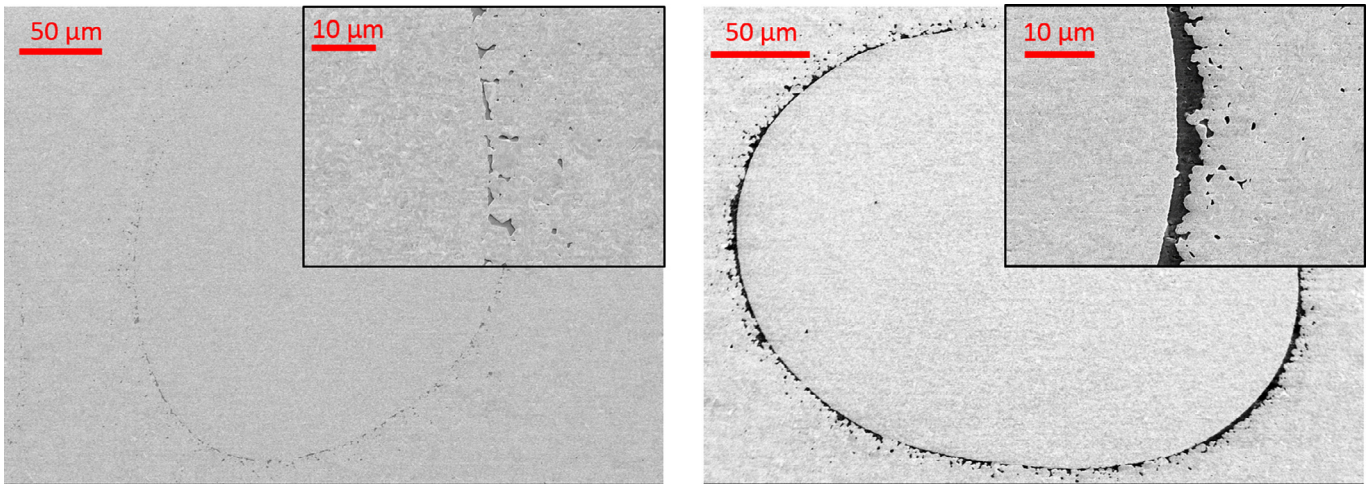

Fig. 11. SEM images of yttrium oxide interface in the actual W_f/W composite after the FAST process: 1 µm thick coating (a); 2.5 µm thick coating.

the stoichiometric composition together with a lattice parameter restoration.

Based on the microstructure characteristics, the poisoned mode thin film was chosen as a candidate for permeation barrier coating, while the metallic mode yttrium oxide thin film was chosen as the candidate of the W_f/W interface material. For both applications, the preliminary test results were promising.

Nevertheless, both deposition modes showed some issues after the annealing process: in metallic mode films, cracks are formed and in poisoned mode thin films, an intermediate oxidation layer is generated. To further increase the thin film quality, two potential solutions are suggested here: 1. Heat the substrate to the aimed temperature during magnetron sputtering [50-54], where the difference in thermal expansion coefficient still needs to be noticed during the cooling of the sample. 2. Deposition with a combined process of both modes. A thin metallic mode thin film can be deposited as an intermediate layer between the poisoned mode layer and the substrate to isolate the reaction between them. At the same time, the thermal expansion force can be redistributed by the high porosity in the poisoned mode layer.

References

[1] J. Zhu, Y. Zhu, W. Shen, Y. Wang, J. Han, G. Tian, P. Lei, B. Dai, Growth and characterization of yttrium oxide films by reactive magnetron sputtering, Thin Solid Films 519 (2011) 4894–4898.

[2] L. Wang, Y. Pan, Y. Ding, W. Yang, W.L. Mao, S.V. Sinogeikin, Y. Meng, G. Shen, H.-k. Mao, High-pressure induced phase transitions of Y_2O_3 and Y_2O_3:Eu^{3+}, Appl. Phys. Lett. 94 (2009) 061921.

[3] S.A. Barve, N.Mithal Jagannath, M.N. Deo, A. Biswas, R. Mishra, R. Kishore, B.M. Bhanage, L.M. Gantayet, D.S. Patil, Effects of precursor evaporation temperature on the properties of the yttrium oxide thin films deposited by microwave electron cyclotron resonance plasma assisted metal organic chemical vapor deposition, Thin Solid Films 519 (2011) 3011–3020.

[4] R. Forrest, A. Tabasso, C. Danani, S. Jakhar, A Shaw, in: Handbook of Activation Data Calculated using EASY-2007, UKAEA FUS, 2009, p. 552.

[5] F. Yan, Z.T. Liu, W.T. Liu, Structural and optical properties of yttrium trioxide thin films prepared by RF magnetron sputtering, Vacuu 86 (2011) 72–77.

[6] B.H. O'Connor, T.M. Valentine, A neutron diffraction study of the crystal structure of the C-form of yttrium sesquioxide, AcCrB 25 (1969) 2140–2144.

[7] M.G. Paton, E.N. Maslen, A refinement of the crystal structure of yttria, Acta Crystallogr. 19 (1965) 307–310.

[8] R.J. Gaboriaud, F. Paumier, M. Jublot, B. Lacroix, Ion irradiation-induced phase transformation mechanisms in Y_2O_3 thin films, Nucl. Instrum. Methods Phys. Res. Sec. B 311 (2013) 86–92.

[9] S. Berg, T. Nyberg, Fundamental understanding and modeling of reactive sputtering processes, Thin Solid Films 476 (2005) 215–230.

[10] P. Lei, J. Zhu, Y. Zhu, C. Jiang, X. Yin, Yttrium oxide thin films prepared under different oxygen-content atmospheres: microstructure and optical properties, Appl. Phys. A 108 (2012) 621–628.

[11] K. Strijckmans, W.P. Leroy, R. De Gryse, D. Depla, Modeling reactive magnetron sputtering: fixing the parameter set, Surf. Coat. Technol. 206 (2012) 3666–3675.

[12] P. Lei, W. Leroy, B. Dai, J. Zhu, X. Chen, J. Han, D. Depla, Study on reactive sputtering of yttrium oxide: process and thin film properties, Surf. Coat. Technol. 276 (2015) 39–46.

[13] I. Safi, Recent aspects concerning DC reactive magnetron sputtering of thin films: a review, Surf. Coat. Technol. 127 (2000) 203–218.

[14] P. Marcus, F.B. Mansfeld, Analytical Methods in Corrosion Science and Engineering, CRC press, 2005.
[15] A.F. Jankowski, Sputter deposition of yttrium–oxides, J. Vacuum Sci. Technol. A 11 (1993) 1548.
[16] S. Van Steenberge, W.P. Leroy, D. Depla, Influence of oxygen flow and film thickness on the texture and microstructure of sputtered ceria thin films, Thin Solid Films 553 (2014) 2–6.
[17] K. Seshan, Handbook of Thin Film Deposition, William Andrew, 2012.
[18] P.B. Barna, M. Adamik, Fundamental structure forming phenomena of polycrystalline films and the structure zone models, Thin Solid Films 317 (1998) 27–33.
[19] Z. Xie, A.M. Allen, M. Chang, P. Wang, T.-j. Gung, Control of bombardment energy and energetic species toward a superdense titanium nitride film, J. Vacuum Sci. Technol. A 28 (2010) 1326–1329.
[20] S. Mahieu, W.P. Leroy, K. Van Aeken, M. Wolter, J. Colaux, S. Lucas, G. Abadias, P. Matthys, D. Depla, Sputter deposited transition metal nitrides as back electrode for CIGS solar cells, SoEn 85 (2011) 538–544.
[21] S. Mahieu, K. Van Aeken, D. Depla, Quantification of the ion and momentum fluxes toward the substrate during reactive magnetron sputtering, J. Appl. Phys. 104 (2008) 113301.
[22] P. Norajitra, Divertor Development for a Future Fusion Power Plant, KIT Scientific Publishing, 2014.
[23] B.D. Cullity, S.R. Stock, Elements of X-Ray Diffraction, 3rd Edition, Prentice Hall, 2001.
[24] P. Scherrer, Bestimmung der Größe und der inneren struktur von kolloidteilchen mittels röntgenstrahlen, nachrichten von der gesellschaft der wissenschaften zu göttingen, Math. Phys. Klasse 2 (1918) 98–100.
[25] B.K. Sarma, A.R. Pal, H. Bailung, J. Chutia, Effect of post-deposition annealing on the growth of nanocrystalline TiO_2 thin films and elastic anisotropy of rutile phase at different temperatures, JAllC 577 (2013) 261–268.
[26] H.J. Quah, K.Y. Cheong, Effects of post-deposition annealing ambient on Y_2O_3 gate deposited on silicon by RF magnetron sputtering, JAllC 529 (2012) 73–83.
[27] M. Szymańska, S. Gierałtowska, Ł Wachnicki, M. Grobelny, K. Makowska, R. Mroczyński, Effect of reactive magnetron sputtering parameters on structural and electrical properties of hafnium oxide thin films, Appl. Surf. Sci. 301 (2014) 28–33.
[28] F. Wang, M.Z. Wu, Y.Y. Wang, Y.M. Yu, X.M. Wu, L.J. Zhuge, Influence of thickness and annealing temperature on the electrical, optical and structural properties of AZO thin films, Vacuu 89 (2013) 127–131.
[29] L.C. Agudelo-Morimitsu, J. De La Roche, D. Escobar, R. Ospina, E. Restrepo–Parra, Substrate heating and post-annealing effect on tungsten/tungsten carbide bilayers grown by non-reactive DC magnetron sputtering, Ceram. Int. 39 (2013) 7355–7365.
[30] Y.-N. Xu, Z.-q. Gu, W.Y. Ching, Electronic, structural, and optical properties of crystalline yttria, PhRvB 56 (1997) 14993–15000.
[31] S. Takayanagi, T. Yanagitani, M. Matsukawa, Unusual growth of polycrystalline oxide film induced by negative ion bombardment in the capacitively coupled plasma deposition, Appl. Phys. Lett. 101 (2012) 232902.
[32] T. Yanagitani, M. Kiuchi, Control of in-plane and out-of-plane texture in shear mode piezoelectric ZnO films by ion-beam irradiation, J. Appl. Phys. 102 (2007) 044115.
[33] P. Souček, T. Schmidtová, L. Zábranský, V. Buršíková, P. Vašina, O. Caha, J. Buršík, V. Peřina, R. Mikšová, Y.T. Pei, J.T.M. De Hosson, On the control of deposition process for enhanced mechanical properties of nc-TiC/a-C: H coatings with DC magnetron sputtering at low or high ion flux, Surf. Coat. Technol. 255 (2014) 8–14.
[34] F. Yang, X. Xiang, G. Lu, G. Zhang, T. Tang, Y. Shi, X. Wang, Tritium permeation characterization of Al_2O_3/FeAl coatings as tritium permeation barriers on 321 type stainless steel containers, J. Nucl. Mater. 478 (2016) 144–148.
[35] Y.P. Xu, S.X. Zhao, F. Liu, X.C. Li, M.Z. Zhao, J. Wang, T. Lu, S.H. Hong, H.S. Zhou, G.N. Luo, Studies on oxidation and deuterium permeation behavior of a low temperature α-Al_2O_3-forming Fe-Cr-Al ferritic steel, J. Nucl. Mater. 477 (2016) 257–262.
[36] T. Chikada, S. Naitoh, A. Suzuki, T. Terai, T. Tanaka, T. Muroga, Deuterium permeation through erbium oxide coatings on RAFM steels by a dip-coating technique, J. Nucl. Mater. 442 (2013) 533–537.
[37] T. Chikada, A. Suzuki, F. Koch, H. Maier, T. Terai, T. Muroga, Fabrication and deuterium permeation properties of erbia-metal multilayer coatings, J. Nucl. Mater. 442 (2013) S592–S596.
[38] T. Chikada, A. Suzuki, T. Tanaka, T. Terai, T. Muroga, Microstructure control and deuterium permeability of erbium oxide coating on ferritic/martensitic steels by metal-organic decomposition, Fusion Eng. Des. 85 (2010) 1537–1541.
[39] J. Engels, A. Houben, M. Rasinski, C. Linsmeier, Yttrium oxide coatings as tritium permeation barriers, Poster SOFT 2016 (P3.180), 2016.
[40] J. Engels, A. Houben, M. Rasinski, C. Linsmeier, Hydrogen saturation and permeation barrier performance of yttrium oxide coatings, Fusion Eng. Des. (2016) submitted.
[41] J. Riesch, Y. Han, J. Almanstötter, J.W. Coenen, T. Höschen, B. Jasper, P. Zhao, C. Linsmeier, R. Neu, Development of tungsten fibre-reinforced tungsten composites towards their use in DEMO - Potassium doped tungsten wire, Phys. Scr. (2016).
[42] B. Jasper, S. Schoenen, J. Du, T. Hoeschen, F. Koch, C. Linsmeier, R. Neu, J. Riesch, A. Terra, J.W. Coenen, Behavior of tungsten fiber-reinforced tungsten based on single fiber push-out study, Nucl. Mater. Energy (2016).
[43] B. Jasper, J.W. Coenen, J. Riesch, T. Höschen, M. Bram, C. Linsmeier, Powder metallurgical tungsten fiber-reinforced tungsten, Mater. Sci. Forum 825-826 (2015) 125–133.
[44] J. Riesch, T. Höschen, C. Linsmeier, S. Wurster, J.H. You, Enhanced toughness and stable crack propagation in a novel tungsten fibre-reinforced tungsten composite produced by chemical vapour infiltration, Phys. Scr. T159 (2014) 014031.
[45] J. Riesch, T. Höschen, C. Linsmeier, S. Wurster, J.H. You, Enhanced toughness and stable crack propagation in a novel tungsten fibre-reinforced tungsten composite produced by chemical vapour infiltration, Phys. Scr. (2014).
[46] J. Riesch, J.Y. Buffiere, T. Höschen, M. di Michiel, M. Scheel, C. Linsmeier, J.H. You, In situ synchrotron tomography estimation of toughening effect by semi-ductile fibre reinforcement in a tungsten-fibre-reinforced tungsten composite system, Acta Mater. 61 (2013) 7060–7071.
[47] C.S. Bonifacio, T.B. Holland, K. Van Benthem, Time-dependent dielectric breakdown of surface oxides during electric-field-assisted sintering, Acta Mater. 63 (2014) 140–149.
[48] C.S. Bonifacio, T.B. Holland, K. van Benthem, Evidence of surface cleaning during electric field assisted sintering, Scr. Mater. 69 (2013) 769–772.
[49] J.W. Coenen, Y. Mao, A. Calvo, S.K. Sistla, B. Jasper, J. Riesch, M. Rieth, G. Pintsuk, F. Klein, A. Litnovsky, A.v. Müller, T. Wegener, J.-H. You, C. Broeckmann, C. Garcia-Rosales, R. Neu, C. Linsmeier, Advanced materials for a damage resilient divertor concept for DEMO, Talk SOFT, 2016, 2016.
[50] P.K. Mishra, V. Dave, R. Chandra, J.N. Prasad, A.K. Choudhary, Effect of processing parameter on structural, optical and electrical properties of photovoltaic chalcogenide nanostructured RF magnetron sputtered thin absorbing films, Mater. Sci. Semicond. Process. 25 (2014) 307–319.
[51] Y.M. Zhou, Z. Xie, H.N. Xiao, P.F. Hu, J. He, Effects of deposition parameters on tantalum films deposited by direct current magnetron sputtering in Ar–O_2 mixture, Appl. Surf. Sci. 258 (2011) 1699–1703.
[52] Z.S. Schiaber, D.M.G. Leite, J.R.R. Bortoleto, P.N. Lisboa-Filho, J.H.D. da Silva, Effects of substrate temperature, substrate orientation, and energetic atomic collisions on the structure of GaN films grown by reactive sputtering, J. Appl. Phys. 114 (2013) 183515.
[53] B.L. Zhu, S.J. Zhu, J. Wang, J. Wu, D.W. Zeng, C.S. Xie, Thickness effect on structure and properties of ZAO thin films by RF magnetron sputtering at different substrate temperatures, Phys. E Low Dimens. Syst. Nanostruct. 43 (2011) 1738–1745.
[54] G. Schmidl, J. Dellith, E. Kessler, U. Schinkel, The influence of deposition parameters on Ti/Pt film growth by confocal sputtering and the temperature dependent resistance behavior using SiOx and Al_2O_3 substrates, Appl. Surf. Sci. 313 (2014) 267–275.